

CHEMISTRY

AN **ASIAN** JOURNAL

www.chemasianj.org

Accepted Article

Title: Plasmon Coupling Induced Hot Electrons for Photocatalytic Hydrogen Generation

Authors: Can Xue, Xu Yuan, Wenlong Zhen, and Sijia Yu

This manuscript has been accepted after peer review and appears as an Accepted Article online prior to editing, proofing, and formal publication of the final Version of Record (VoR). This work is currently citable by using the Digital Object Identifier (DOI) given below. The VoR will be published online in Early View as soon as possible and may be different to this Accepted Article as a result of editing. Readers should obtain the VoR from the journal website shown below when it is published to ensure accuracy of information. The authors are responsible for the content of this Accepted Article.

To be cited as: *Chem. Asian J.* 10.1002/asia.202100856

Link to VoR: <https://doi.org/10.1002/asia.202100856>

A Journal of



A sister journal of *Angewandte Chemie*
and *Chemistry – A European Journal*

WILEY-VCH

FULL PAPER

Plasmon Coupling Induced Hot Electrons for Photocatalytic Hydrogen Generation

Xu Yuan,^[a] Wenlong Zhen,^[a] Sijia Yu,^[a] and Can Xue^{*[a]}

[a] X. Yuan, Dr. W. Zhen, Dr. S. Yu, Prof. Dr. C. Xue
School of Materials Science and Engineering
Nanyang Technological University
50 Nanyang Avenue, 639798, Singapore
E-mail: cxue@ntu.edu.sg

Abstract: We present the fabrication of core-shell-satellite Au@SiO₂-Pt nanostructures and demonstrate that LSPR excitation of the core Au nanoparticle can induce plasmon coupling effect to initiate photocatalytic hydrogen generation from decomposition of formic acid. Further studies suggest that the plasmon coupling effect induces strong local electric field between the Au core and Pt nanoparticles on the SiO₂ shell, which enables creation of hot electrons on the non-plasmonic-active Pt nanoparticles to participate hydrogen evolution reaction on the Pt surface. In addition, small SiO₂ shell thickness is required in order to obtain strong plasmon coupling effect and achieve efficient photocatalytic activities for hydrogen generation.

Introduction

The electron cloud of noble metal nanoparticles (NPs) oscillates coherently upon illumination of incident light, this phenomenon is known as localized surface plasmon resonance (LSPR).^[1] This unique process allows plasmonic nanostructures to harvest the energy of light and convert it into heat and energetic charge carriers. Therefore, noble metal NPs have been widely used in a wide range of fields, including bio-imaging,^[2] cancer therapy,^[3] drug delivery,^[4] optical device,^[5] and catalysis.^[6] Among these applications, photocatalysis utilizing the LSPR of plasmonic metal materials can be a promising solution for efficiently utilizing solar energy. To figure out the contribution of LSPR to photocatalytic reactions, some dominant mechanisms have been proposed, including photothermal effect,^[7] excitation of hot electrons,^[8] and enhanced local electric field.^[9] However, the synergistic effect between these mechanisms remains elusive.

Researchers have revealed that LSPR excitation can induce several non-mutually exclusive processes to assist the photocatalytic reactions. First, heat is generated when plasmonic nanostructures absorb light, which results in increasing local temperature and accelerates reaction rates.^[10] Note that the size of NPs can affect the photothermal efficiency, and the optimum size is about 40~60 nm.^[7b] Second, the enhanced electric field confined on the metal surface, resulting from electronic oscillation upon illumination, increases the available amount of photons, and consequently promote proximal photochemical reactions.^[11] Third, hot electrons, arising from non-radiative decay of localized surface plasmon excitation, could transfer to the adsorbate molecules or contacted particles to facilitate the related reactions.^[7a, 8a]

Hot electrons play critical roles in catalytic reactions, but have problems of limited amount of high-energy electrons^[12] and short lifetime.^[13] Previous studies have suggested that amount of hot electrons increases significantly in proximity to the places with

stronger local electric field,^[14] though the mechanism behind this mutual effect is still elusive. To verify the hypothesis, a significantly enhanced local electric field is needed, which may be realized by placing two plasmonic NPs in proximity. Plasmon coupling occurs when plasmon oscillation of the two NPs interacts with each other.^[15] Indeed, the plasmon coupling effect does not require both metal NPs being capable of LSPR excitation by the incident light.^[16] It means that a plasmon coupled structure with only one component having LSPR absorption can possibly create hot electrons on the non-plasmonic-active component, where the catalytic reaction could be initialized through plasmon coupling under light excitation.

Herein, in order to verify this hypothesis, we have fabricated core-shell-satellite Au@SiO₂-Pt nanostructures for photocatalytic hydrogen evolution in formic acid for proof-of-concept. We have found that the Au@SiO₂-Pt nanostructure exhibits significantly enhanced photocatalytic activities as compared with the control samples without either Au cores or decorated Pt nanoparticles on the SiO₂ shell. Further studies suggest that the promoted photocatalytic activities of Au@SiO₂-Pt is owing to the Pt hot electrons that are inductively created from plasmon coupling between the Au core and Pt nanoparticles on the silica shell. Moreover, the silica shell thickness plays a crucial role for plasmon coupling, and significantly influences the photocatalytic activities of the core-shell-satellite Au@SiO₂-Pt nanostructures.

Results and Discussion

To obtain the core-shell-satellite Au@SiO₂-Pt nanostructure, Au NPs were firstly synthesized. TEM examinations (Figure 1a) revealed that the average diameter of the as-prepared Au nanoparticles was 67.6±5.7 nm. Subsequently, silica-coating was applied to the Au NPs. By using 0.1 mM TEOS in the sol-gel process, the obtained SiO₂ shell thickness is around 3 nm (Figure 1b). When the TEOS concentration increased to 0.3 mM and 1 mM, the SiO₂ shell thickness changed to 10 nm and 18 nm, respectively (Figure 1c, d).

Finally, Pt NPs with the size of 2~3 nm (Figure 2) were deposited onto the surface of silica-coated Au (Au@SiO₂) NPs. The composition of the Au@SiO₂-Pt nanostructure was verified by EDX mapping (Figure 3). The in-situ decoration of Pt NPs on the SiO₂ shell could be ascribed to the SPR excitation of the Au core and the consequent high temperature localized on the SiO₂ surface to initiate reduction of K₂PtCl₄ by isopropanol. The quantitative elemental composition was identified by inductive coupled plasma optical emission spectrometry (ICP-OES) with the Au to Pt atomic ratio as 25.08:1.

FULL PAPER

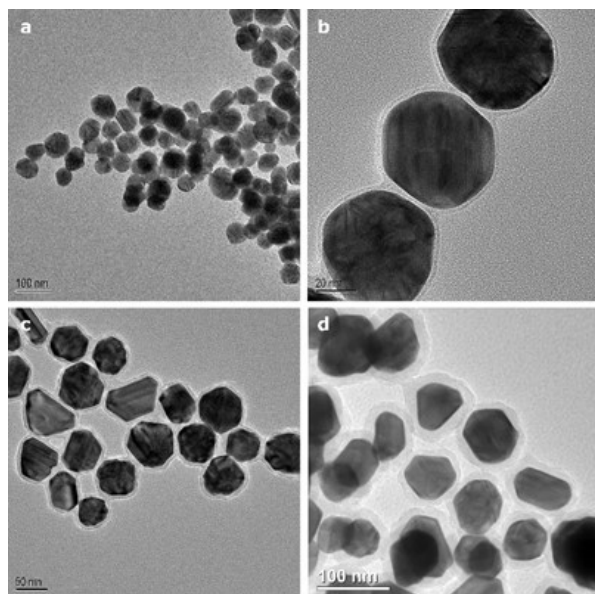


Figure 1. TEM images of (a) Au NPs and Au@SiO₂ NPs with silica shell thickness of (b) 3nm, (c) 10nm, and (d) 18nm.

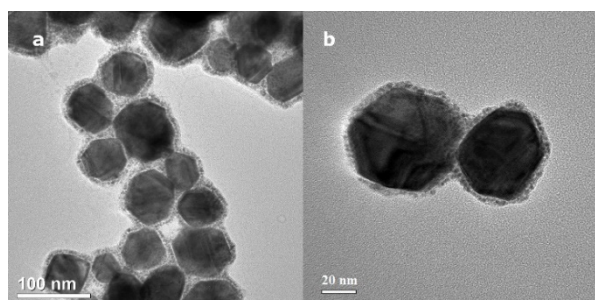


Figure 2. TEM images of Au@SiO₂-Pt (3 nm SiO₂ shell thickness).

The UV-vis analyses showed dramatic change upon Pt nanoparticle decoration. As shown in Figure 4, the normalized UV-vis spectrum of Au@SiO₂ NPs presented a sharp LSPR peak at 543 nm. After photodeposition of Pt, the LSPR peak redshifts drastically to 686 nm, which can be attributed to the plasmon coupling between the Au core and Pt NPs on the SiO₂ shell.

When two metal nanoparticles are placed in proximity, plasmon coupling is established through strong interaction between their plasmon oscillations. This plasmon coupling modulates the LSPR frequency of the plasmon coupling nanostructures. Generally, a favorable coupling of the plasmon resonance of the coupled nanoparticles requires lower frequency to drive the coupled plasmon resonance, which leads to redshift of plasmon band.^[15c] Previous researchers have demonstrated that the redshift of the LSPR peak is strong evidence for plasmon coupling. For example, the plasmon coupling between 88 nm gold nanodisc pair with 2 nm interparticle distance (polarized along interparticle axis) led to a redshift of ~84 nm as compared to the plasmon band of isolated gold nanodisc, which was only 561 nm.^[17] When individual Au-Ag@SiO₂ heterodimer was polarized parallel to dimer axis, the plasmon coupling

between Au and Ag also led to comparable redshift of the two dimer resonances.^[18]

For the presented Au@SiO₂-Pt nanostructures with 3 nm silica shell thickness, the LSPR peak shifted dramatically from 543nm to 686 nm, which is a strong evidence of intense plasmon coupling between the Au and Pt nanoparticles.^[15c, 17-18] The shoulder peak at ~540 nm might be due to the Au@SiO₂-Pt particles with very low surface density of Pt nanoparticles. Because the 3 nm silica shell is too thin to be condensed, on some Au@SiO₂ nanoparticles, the surface adsorption of [PtCl₄]²⁻ ions might be fairly weak, which resulted in low photodeposition density of Pt. Consequently, the influence of plasmon coupling on the core Au nanoparticle becomes very weak with almost no spectral shift.

For a proof-of-concept application, the Au@SiO₂-Pt nanostructures (3 nm SiO₂ shell thickness) were used as the photocatalyst for visible-light-driven hydrogen generation in the formic acid solution. As shown in Figure 5, the Au@SiO₂-Pt sample presented steady H₂ evolution under visible light irradiation, while the control samples, the Au NPs, Au@SiO₂ NPs, and Pt decorated SiO₂ (SiO₂-Pt) NPs showed no activities (Figure S1). In a further control experiment, the Au@SiO₂-Pt sample was placed in formic acid in dark at 70°C, and no H₂ evolution was observed, which allowed us to exclude the photothermal effect from LSPR excitation of Au.

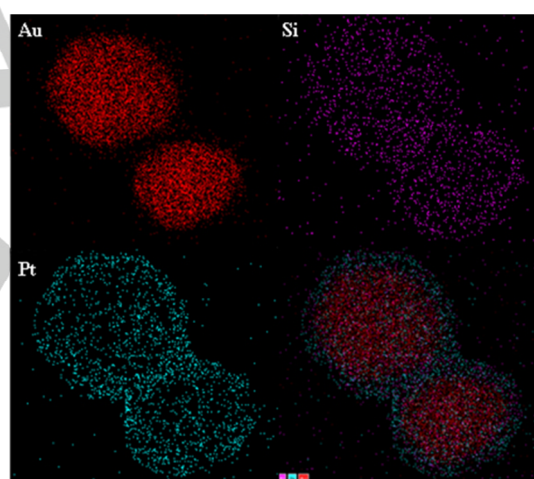


Figure 3. EDX mapping of Au@SiO₂-Pt to show the distribution of the elements Au, Si and Pt.

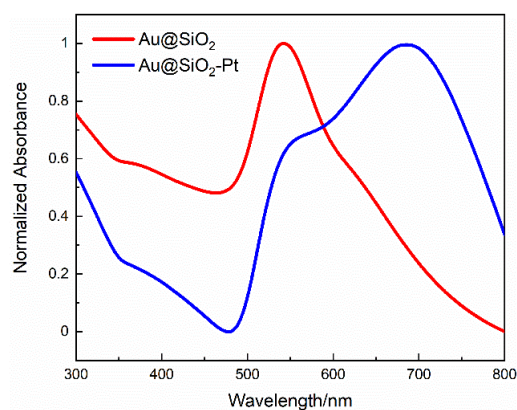


Figure 4. UV-Vis Spectra of Au@SiO₂ and Au@SiO₂-Pt nanoparticles.

FULL PAPER

These results suggest that the H_2 evolution occurred on the surface of Pt NPs which are inactive to visible light. The Au core is responsible to harvesting the visible light, but LSPR excitation of individual Au NPs could not initiate the H_2 evolution reaction. Although hot electrons could be generated on Au upon LSPR excitation, these electrons could not transport through the insulating SiO_2 shell to Pt NPs for chemical reactions. The only source for hot electrons generation was Pt NPs. As such, we could hypothesize that the visible light irradiation induces plasmon coupling between the Au core and Pt NPs on SiO_2 shell and creates strong local electric field that enables generation of hot electrons on the Pt NPs to initiate H_2 evolution reaction. The proposed reaction mechanism is depicted in Figure 6.

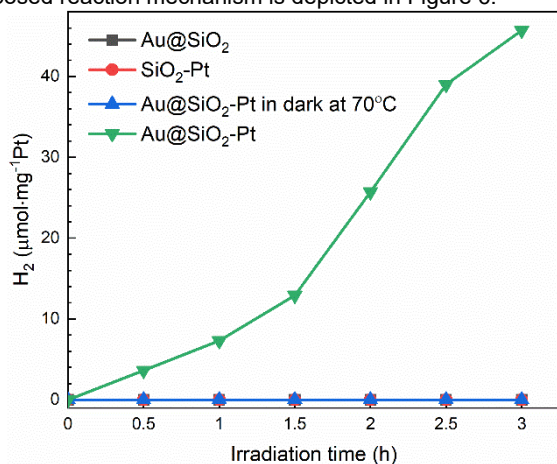


Figure 5. Photocatalytic hydrogen evolution amount over different samples.

In the proposed model, the plasmon coupling involves both plasmonic Au NP and non-plasmonic Pt NP. The hot electrons generated on Pt still originate from the LSPR excitation of the plasmonic Au NP. In order to further verify the contribution from LSPR excitation of Au, we compared the photocatalytic activities of the Au@SiO₂-Pt (3 nm SiO₂ shell thickness) under irradiation of two different wavelengths, 430±10 nm and 600±10 nm, with the same light intensity. As shown in Figure 7, the stronger plasmonic excitation at 600±10 nm results in much higher H_2 evolution rate than weak excitation at 430±10 nm in spite of higher photon energy of 430 nm light. This clearly support that the stronger LSPR excitation allows for more effective generation of hot electrons on Pt towards higher photocatalytic activities.

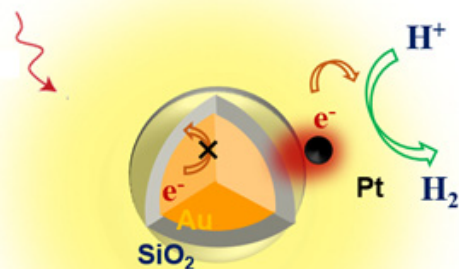


Figure 6. Possible photocatalytic reaction mechanism.

Since the plasmon coupling effect is critical dependent on the interparticle distance as the intensity of local electric field decays with distance r away from the particle as $1/r^3$,^[19] the silica shell thickness in this work becomes an important factor to manage the local electric field between the Au core and surface Pt NPs. By varying the TEOS concentration in the silica coating procedures, we could obtain different SiO₂ shell thickness including 3 nm, 10 nm and 18nm. Then the same protocol of Pt photodeposition was applied for decoration of Pt NPs onto the silica shell. The same amount of Pt precursor was used for these three samples. Figure 8 shows the Au@SiO₂-Pt samples with the silica shell thickness of 10 nm and 18 nm.

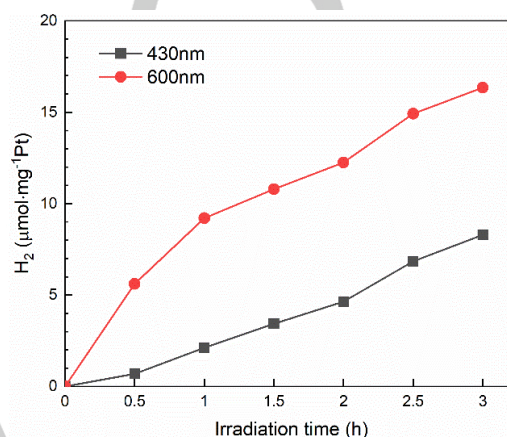


Figure 7. Photocatalytic hydrogen evolution over Au@SiO₂-Pt under incident light with different wavelength.

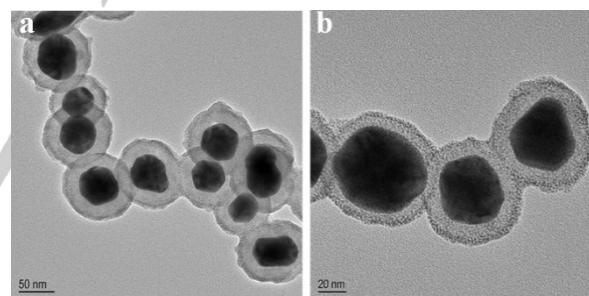


Figure 8. TEM images of Au@SiO₂-Pt with silica shell thickness of (a) 18nm, (b) 10nm.

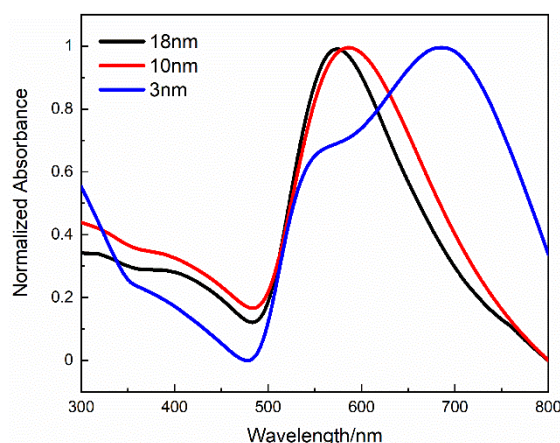


Figure 9. UV-Vis spectra of Au@SiO₂-Pt with different silica shell thickness

FULL PAPER

The UV-vis spectra (Figure 9) show relatively minor shift upon Pt NP decoration for the samples with 10 nm and 18 nm shell thickness, suggesting weak plasmonic coupling in these two Au@SiO₂-Pt samples since the interaction between Au core and Pt nanoparticles decreased with enlarged distance.^[15c, 17, 20] The visible light photocatalytic test showed more than 9 times lower H₂ evolution activities for these two samples as compared to the Au@SiO₂-Pt with 3 nm shell thickness. Note that without silica shell (0 nm shell thickness), the resulted Au@Pt nanoparticles (Figure S2) showed no photocatalytic activity because the directly attached Pt on Au strong damping of Au LSPR. The FDTD simulation results, as shown in Figure S3, also indicate larger redshift of the LSPR band as the silica shell thickness decreases, which is consistent with the experimental observations.

The above results suggest that at increasing Au-Pt interparticle distance, the plasmon coupling effect becomes very weak, and the intensity of local electric field between Au core and Pt nanoparticles decreases dramatically. Govorov et al. have previously demonstrated that intensity of plasmonic field directly correlated with the generation rate of hot electrons.^[21] In particular for plasmon coupling system, the strongly enhanced local electric field in the gap region allows for drastically increased rate of hot electron generation on the involved nanoparticle surfaces.^[22] Therefore in our studies, increased silica shell thickness resulted in weaker plasmon coupling and consequently lower intensity of local field. The FDTD simulation results (Figure S4) reveal that for the Au@SiO₂-Pt with 3 nm shell thickness, strong local electric field is present on both Au and Pt particles in the gap region. While for the Au@SiO₂-Pt with 10 nm and 18 nm shell thickness, the local electric field on Pt becomes much weaker, which led to reduced capability of hot electrons on Pt and thus decreased photocatalytic activities. From this point of view, our observation suggests that small interparticle distance is ultimately important to achieve strong Au-Pt plasmon coupling and intense local electric field for hot electron generation on the non-plasmonic Pt nanoparticles.

Conclusion

In conclusion, we have synthesized Au@SiO₂-Pt core-shell-satellite nanostructures and used this model structure to demonstrate that plasmon coupling between the Au core and the Pt NPs on the silica shell could initiate H₂ evolution reaction in formic acid solution. Further analyses suggest that the Au-Pt plasmon coupling may create strong local electric field that enables hot electron generation on Pt NPs to participate the decomposition of formic acid towards H₂ evolution. This work is of importance because it presents a new route to initiate photocatalytic reactions on non-plasmonic nanoparticles by creating hot electrons through plasmon coupling effect.

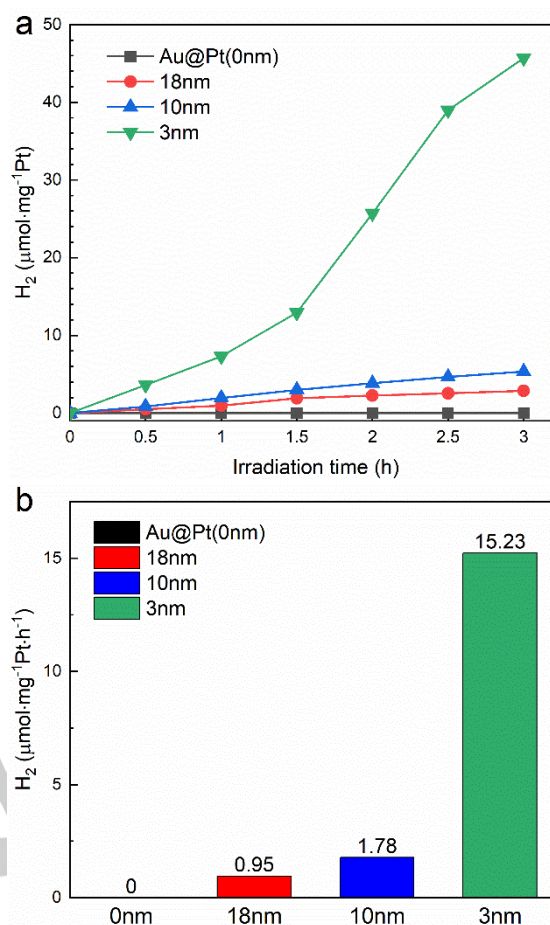


Figure 10. (a) Photocatalytic hydrogen evolution amount over the Au@SiO₂-Pt samples with different silica shell thickness versus visible light irradiation time; (b) The average H₂ evolution rate over 3 hours for the samples. The Au@SiO₂-Pt-3nm sample showed an H₂ evolution amount of 45.7 μmol/mg_{Pt} in 3 hours, which is much higher than Au@SiO₂-Pt-10nm (5.3 μmol/mg_{Pt}), Au@SiO₂-Pt-18nm (2.9 μmol/mg_{Pt}) and Au@Pt (0 μmol/mg_{Pt}). As for Au@Pt, noted that Pt nanoparticles were directly deposited onto Au nanoparticles without silica coating (Figure S2).

Experimental Section

Materials

Gold(III) chloride hydrate (HAuCl₄, ≥49.0%, Au Basis), tri-sodium citrate (Na₃Ci, 99%), ethanol (99%), tetraethyl orthosilicate (TEOS, 98%), 16-mercaptohexadecanoic acid (MHA, 90%), hexachloroplatinic (IV) acid hexahydrate (H₂PtCl₆·6H₂O) Potassium tetrachloroplatinate(II) (K₂PtCl₄, 98%), 3-aminopropyltriethoxysilane (APTES, 99%), ammonium hydroxide solution (30-33% NH₃ in H₂O), sodium dodecyl sulfate (SDS, ≥99.0%), formic acid (≥96%) and hydrochloric acid fuming (37%) were all purchased from Sigma-Aldrich. Isopropyl alcohol (≥99.8%) was purchased from Fisher Chemical. Tetraisopropyl orthosilicate (>99.0%) was purchased from TCI. Nitric acid (≥96%) was purchased from Honeywell Fluka. All glassware were washed with aqua regia, HCl: HNO₃=3:1 (v:v), and rinsed with ethanol and Milli-Q water. Deionized water (18.2 kΩ·cm, Milli-Q System, Millipore, Billerica) was used in all the experiments. All the chemical reagents were used as received without further purification.

FULL PAPER

Characterizations

TEM examinations were carried out on a JEOL 2100F transmission electron microscope operated at 200kV. UV-vis absorption spectra were recorded on Shimadzu UV-1800 UV-Vis spectrophotometer. The gold and platinum content were measured by inductive coupled plasma on an iCAP6200DUO ICP-OES spectrometer (Thermo Fisher Scientific).

Sample preparation

Synthesis of gold nanoparticles. The gold nanoparticles were synthesized using a seed-mediated method. The gold seeds were prepared by injecting 5 mL NaCl solution (38.8 mM) into 50 mL boiling HAuCl₄ solution (1 mM) under vigorous stirring. The reaction was kept boiling for 15 min and then cooled to room temperature for later use as the seeds.

Next, 3 mL HAuCl₄ solution (50mM) were added into 247 mL water in a 500mL round bottom flask. Then 2.25 mL as-prepared Au seeds solution and 5 mL NaCl solution (38.8 mM) were injected into the flask in sequence after the mixture was boiling. After 30 min, 10 mL NaCl solution (38.8 mM) was added into the flask as stabilizer. Then the mixture was kept boiling for 1 hour. After the reaction completed, the products were separated via centrifugation, and re-suspended in 0.3 mM NaCl solution.

Silica coating of Au nanoparticles. Silica coating was conducted through a modified Stöber method. Typically, 0.25 mL ethanol solution of MHA (10mM) was added into 2.5 mL as-prepared solution of Au nanoparticles in a 20-mL glass vial. After 30 min, 10 mL TEOS solution (0.1275 mM in IPA) was added to vial under vigorous stirring. After 15 min, 0.25 mL NH₃·H₂O was added to the mixture. After 2 hours, 0.1 mL tetraisopropyl orthosilicate solution (13 mM in IPA) was added to the mixture slowly. After 3 hours, the products were collected via centrifugation and washed with IPA and re-suspended in DI water. For the Au@SiO₂ nanoparticles with different silica shell thickness (3 nm, 10 nm and 18nm), the concentration of TEOS in the mixture was tuned to 0.1 mM, 0.3 mM and 1 mM, respectively.

Photodeposition of Pt NPs onto Au@SiO₂ nanostructures. Typically, 6.5 mL solution of as-prepared Au@SiO₂ nanoparticles was mixed with 13.5 mL IPA and 0.2 mL K₂PtCl₄ (10 mM) in a 35-mL quartz vial. A 300-W Xenon lamp was used as the light source. The quartz vial was irradiated by full range light (240 mW/cm²) for 2 hours under mild stirring before the products were collected via centrifugation.

Measurement of photocatalytic activities

The photocatalytic activities of H₂ generation from decomposition of formic acid in solution were evaluated by using aforementioned samples as photocatalysts. Typically, 2.2mg as-prepared samples were dispersed into 10 mL DI water containing 100μL of formic acid solution (98%). A 20-mL sealed glass vial was used as reactor and purged with Argon for 15 min to remove residual air. A 300 W Xenon lamp (MAX-302, Asahi Spectra Company, Ltd.) coupled with a 420-nm cutoff filter was used as the visible light source. The solution temperature was maintained as the same as ambient condition (~25°C). Reaction kinetics were monitored via analyses of the withdrawn gaseous samples at a

given period using gas chromatography (Agilent 7890A, TCD, 13 X columns, Ar carrier) and gas chromatography (Shimadzu 2010) equipped with FID and TCD detectors.

More experimental details, including synthetic methods, numerical simulation and characterizations are presented in the Supporting Information.

Acknowledgements

This work is supported by the Ministry of Education, Singapore, under AcRF-Tier2 (MOE2018-T2-1-017) and AcRF-Tier1 (MOE2019-T1-002-012, RG102/19). The authors also thank the support from NTU seed funding for Solar Fuels Laboratory.

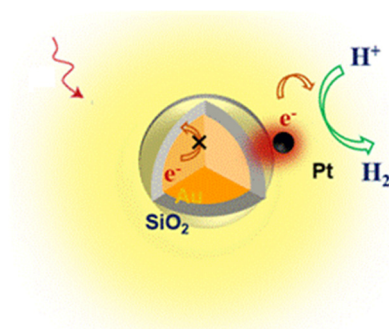
Keywords: plasmon coupling • hot electrons • photocatalytic hydrogen generation • energy transfer

- [1] a) E. Hutter, J. H. Fendler, *Advanced materials* **2004**, *16*, 1685-1706; b) K. L. Kelly, E. Coronado, L. L. Zhao, G. C. Schatz, ACS Publications, **2003**; c) K. L. Kelly, E. Coronado, L. L. Zhao, G. C. Schatz, *Journal of Physical Chemistry B* **2003**, *107*, 668-677.
- [2] a) B. P. Timko, T. Dvir, D. S. Kohane, *Advanced materials* **2010**, *22*, 4925-4943; b) E. Boisselier, D. Astruc, *Chemical society reviews* **2009**, *38*, 1759-1782.
- [3] a) S. D. Brown, P. Nativo, J.-A. Smith, D. Stirling, P. R. Edwards, B. Venugopal, D. J. Flint, J. A. Plumb, D. Graham, N. J. Wheate, *Journal of the American Chemical Society* **2010**, *132*, 4678-4684; b) P. Cherukuri, E. S. Glazer, S. A. Curley, *Advanced drug delivery reviews* **2010**, *62*, 339-345.
- [4] A. S. Urban, T. Pfeiffer, M. Fedoruk, A. A. Lutich, J. Feldmann, *ACS nano* **2011**, *5*, 3585-3590.
- [5] L. Eurenium, C. Högglund, E. Olsson, B. Kasemo, D. Chakarov, *Nature Photonics* **2008**, *2*, 360.
- [6] a) S.-W. Cao, Z. Yin, J. Barber, F. Y. Boey, S. C. J. Loo, C. Xue, *ACS applied materials & interfaces* **2011**, *4*, 418-423; b) Z. Zhang, Z. Wang, S.-W. Cao, C. Xue, *The Journal of Physical Chemistry C* **2013**, *117*, 25939-25947; c) W. Zhen, X. Yuan, X. Shi, C. Xue, *Chemistry-An Asian Journal* **2020**, *15*, 2480-2486; d) W. Zhen, J. Sun, X. Ning, X. Shi, C. Xue, *Applied Catalysis B: Environmental* **2021**, 120568.
- [7] a) G. Baffou, R. Quidant, *Chemical Society Reviews* **2014**, *43*, 3898-3907; b) G. Baffou, H. Rigneault, *Physical Review B* **2011**, *84*, 035415; c) A. Gaiduk, P. V. Ruijgrok, M. Yorulmaz, M. Orrit, *Chemical Science* **2010**, *1*, 343-350.
- [8] a) M. J. Kale, T. Avanesian, P. Christopher, *Acs Catalysis* **2013**, *4*, 116-128; b) S. Sarina, H. Y. Zhu, Q. Xiao, E. Jaatinen, J. Jia, Y. Huang, Z. Zheng, H. Wu, *Angewandte Chemie International Edition* **2014**, *53*, 2935-2940; c) M. L. Brongersma, N. J. Halas, P. Nordlander, *Nature nanotechnology* **2015**, *10*, 25-34; d) J. Li, S. K. Cushing, P. Zheng, T. Senty, F. Meng, A. D. Bristow, A. Manivannan, N. Wu, *Journal of the American Chemical Society* **2014**, *136*, 8438-8449.
- [9] a) Y. Yang, J. Liu, Z.-W. Fu, D. Qin, *Journal of the American Chemical Society* **2014**, *136*, 8153-8156; b) Y. Tsuboi, R. Shimizu, T. Shoji, N. Kitamura, *Journal of the American Chemical Society* **2009**, *131*, 12623-12627.
- [10] N. J. Hogan, A. S. Urban, C. Ayala-Orozco, A. Pimpinelli,

FULL PAPER

- P. Nordlander, N. J. Halas, *Nano letters* **2014**, *14*, 4640-4645.
- [11] a) U. Aslam, V. G. Rao, S. Chavez, S. Linic, *Nature Catalysis* **2018**, *1*, 656-665; b) X.-C. Ma, Y. Dai, L. Yu, B.-B. Huang, *Light: Science & Applications* **2016**, *5*, e16017-e16017.
- [12] R. Sundararaman, P. Narang, A. S. Jermyn, W. A. Goddard III, H. A. Atwater, *Nature communications* **2014**, *5*, 5788.
- [13] Y. Zhang, S. He, W. Guo, Y. Hu, J. Huang, J. R. Mulcahy, W. D. Wei, *Chemical reviews* **2017**, *118*, 2927-2954.
- [14] H. Harutyunyan, A. B. Martinson, D. Rosenmann, L. K. Khorashad, L. V. Besteiro, A. O. Govorov, G. P. Wiederrecht, *Nature nanotechnology* **2015**, *10*, 770.
- [15] a) E. Hao, G. C. Schatz, *The Journal of chemical physics* **2004**, *120*, 357-366; b) W. Rechberger, A. Hohenau, A. Leitner, J. Krenn, B. Lamprecht, F. Ausselegg, *Optics communications* **2003**, *220*, 137-141; c) P. K. Jain, M. A. El-Sayed, *Chemical Physics Letters* **2010**, *487*, 153-164.
- [16] T. Tumkur, X. Yang, C. Zhang, J. Yang, Y. Zhang, G. V. Naik, P. Nordlander, N. J. Halas, *Nano letters* **2018**, *18*, 2040-2046.
- [17] P. K. Jain, W. Huang, M. A. El-Sayed, *Nano Letters* **2007**, *7*, 2080-2088.
- [18] A. Lombardi, M. P. Grzelczak, A. Crut, P. Maioli, I. Pastoriza-Santos, L. M. Liz-Marzan, N. Del Fatti, F. Vallée, *ACS nano* **2013**, *7*, 2522-2531.
- [19] a) P. K. Jain, S. Eustis, M. A. El-Sayed, *The Journal of Physical Chemistry B* **2006**, *110*, 18243-18253; b) D. Griffiths, *Introduction to Electrodynamics* Prentice-Hall, Upper Saddle River, NJ, **1999**.
- [20] K.-H. Su, Q.-H. Wei, X. Zhang, J. Mock, D. R. Smith, S. Schultz, *Nano letters* **2003**, *3*, 1087-1090.
- [21] H. Zhang, A. O. Govorov, *The Journal of Physical Chemistry C* **2014**, *118*, 7606-7614.
- [22] L. V. Besteiro, X.-T. Kong, Z. Wang, G. Hartland, A. O. Govorov, *Acs Photonics* **2017**, *4*, 2759-2781.

Table of Contents



The Au@SiO₂-Pt core-shell-satellite structure was synthesized, and used to demonstrate that hot electrons generated on Pt nanoparticles induced by plasmon coupling between the Au core and the Pt NPs on the silica shell could initiate H₂ evolution reaction in formic acid solution.